15 MILLINEWTON FORCE, 1 MILLIMETER DISPLACEMENT, LOW-POWER MEMS GRIPPER

Craig B. Schindler, Hani C. Gomez*, Dillon Acker-James,*
Daniel Teal, Wei Li, and Kristofer S. J. Pister
Berkeley Sensor & Actuator Center
Department of Electrical Engineering and Computer Sciences
University of California, Berkeley, California, USA

ABSTRACT

We demonstrate a MEMS gripper with a measured 15mN of gripping force over the full gripping displacement of 0 to 1 mm. Integrated contact and capacitive force sensing have been demonstrated and characterized. The gripper has successfully held and released a 0.2 gram through-hole resistor. The integrated electrostatic inchworm motors burn only leakage current (estimated <1 nA) when holding position (gripping or open) and an estimated 0.3 mW when closing at 1 mm/s.

KEYWORDS

electrostatic, inchworm, motor, gripper, microgripper

INTRODUCTION

Microgrippers have been popular applications of MEMS technology for years. A recent survey [1] of 78 different operational strategies adopted in microgrippers shows many designs which include one or more features from the set of low-power consumption, large gripping size, large force, and small size, but none which include all four. For applications such as microrobotics, all are required. One example of a gripper [2] using an electrostatic actuator can grip objects at most 130µm wide with 350µN force, but is over 6.2x3.5x0.8mm^3 (low force to area ratio relative to the grippers presented in this work). Another example using electrostatic actuators is limited to objects at most 100µm wide [3]. Grippers that use thermal actuators, e.g., SMAs, are capable of a much larger gripping force, but at the expense of large electrical power draw (e.g., 130mN at 3000mW [4]). Piezoelectrics, like most electrostatic actuators, can operate with low-power, but also have low actuation distance; these are typically used at centimeter scales with a mechanical reduction for micromanipulation (43x29x5mm, [5]), a setup which is too bulky for a microrobot. Our microgripper, Figure 1, making use of improved high-force low-power angled arm electrostatic inchworm electrostatic motors [6], achieves a 1mm grip at 15mN in an 11x9x0.6 mm^3 form factor.

SYSTEM DESIGN

In total, four MEMS grippers (Figure 2) were designed and fabricated using a three mask silicon-on-insulator (SOI) process. The first mask patterns a 0.5µm e-beam evaporated gold layer, the second mask the 40µm silicon device layer, and the third mask the 550µm silicon substrate. The gold is defined using liftoff, and both the device layer silicon and substrate silicon are etched using deep reactive ion etching (DRIE). A timed vapor HF etch is used to release the device layer structures.

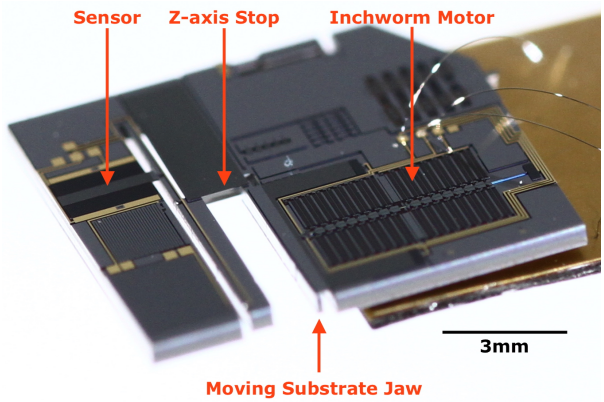

Figure 1: The MEMS gripper on a custom flex circuit board with wirebonds interfacing it to an off-chip control circuit.

The grippers' jaws are actuated by a record high-force angled-arm electrostatic inchworm motor (Figures 3, 4) using 32 gap closing actuators each with 96 moving capacitive fingers (>3000 total moving fingers) [6]. These motors are an optimized, high-force version of the motor described in [7]. The movable jaws are made from an etched piece of the 550µm thick silicon substrate, each attached to the output shuttle of their electrostatic inchworm motor. Restoring springs retract the jaws when the gripped object is released. Capacitive force and resistive contact sensors (Figures 1, 3) are integrated to detect when the devices grasp an object. Z-axis stops (Figures 1, 3, 8) prevent unwanted out of plane motion of the jaws and motor shuttles attached to the motors. The grippers in Figure 2 were designed to hold objects up to 1mm (B, C), 2mm (A), and 3mm (D) wide.

EXPERIMENTAL RESULTS

A top down view of the 11x9x0.6mm^3 gripper B

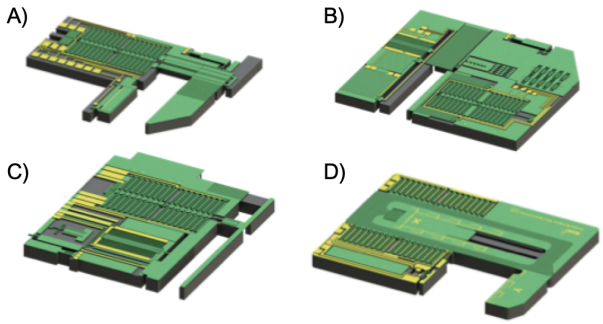

Figure 2: CAD 3D models of the four fabricated and tested SOI MEMS grippers. Green is SOI, dark gray is substrate, and yellow is gold on SOI.

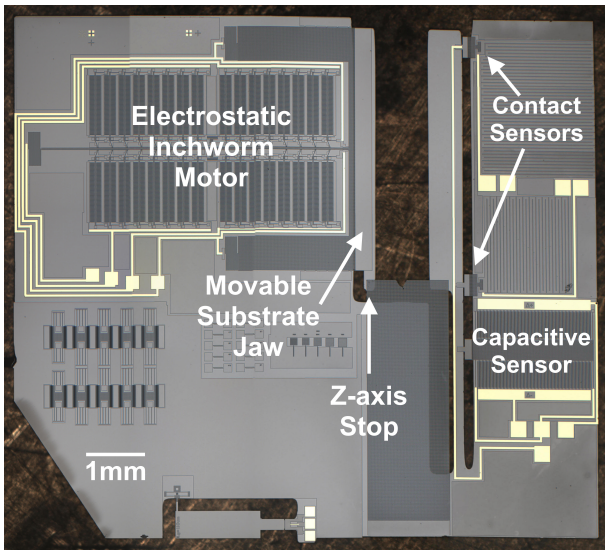

Figure 3: A top-down microscope view of the MEMS gripper B system. Note that the jaw travel distance is 1mm. Subsystems include the high-force motor and various on-chip sensors.

and its subsystems can be seen in Figure 3. The high force motor pushes the shuttle to the right, in the direction of the sensors used to detect opening and closing. This gripper was the most successful and reliable of all four designs.

Additionally, a top down view of the 9.8x7.6x0.6mm^3 gripper D can be seen in Figure 4. Gripper D is designed to have its motor pull its jaw rather than push its jaw. Gripper D is also designed to displace 3mm and has a wider motor shuttle than gripper B. The wider motor shuttle allows for the z-axis stop to be integrated directly into the motor shuttle rather than just with the jaw.

High Force Electrostatic Inchworm Motors

All four grippers were designed using the same electrostatic inchworm motor design. The only variation is the shuttle width in gripper D, in which the two halves of the motor have been moved much farther apart to accommodate a much wider output shuttle. The motor on the grippers has been measured to produce 15mN of force

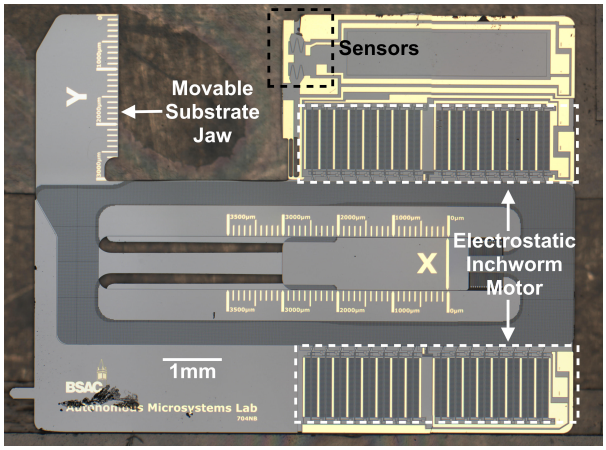

Figure 4: A top-down microscope view of the MEMS gripper D system. Note that the jaw travel distance is 3mm.

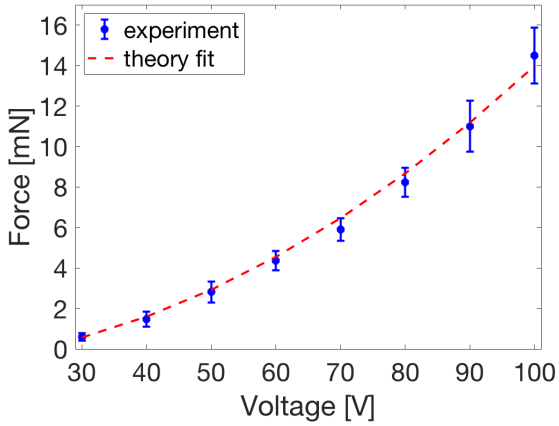

Figure 5: Measured force vs. voltage of the electrostatic inchworm motor on the grippers.

at 100V (Figure 5). The maximum speed of the motor thus far tested is 1mm/s. Force vs. voltage was calculated using the optically measured displacements of springs attached to test structure motors. The spring constant of the springs was calibrated using a Dage 4000 wirebond tester. The device layer DRIE undercut in large SOI trenches was determined to be 0.48µm, calculated by finding the discrepancy between the drawn spring beam width and the actual spring beam width required to match the measured spring constant with theory. The theory fit curve was generated by doing a least squares error minimization of the data to an electrostatic inchworm motor force curve [7] when varying the pawl-to-shuttle engagement distance, which was determined to be 3.4µm. The pawl-to-shuttle distance was drawn in layout as 3µm.

1mm, 2mm and 3mm Jaw Displacement

Figure 6 shows an image of gripper B open and closed with 1mm displacement. In addition to gripper B, grippers A and D have successfully displaced their jaws a distance of 2mm and 3mm, respectively. Figure 7 shows gripper D open and closed with 3mm displacement.

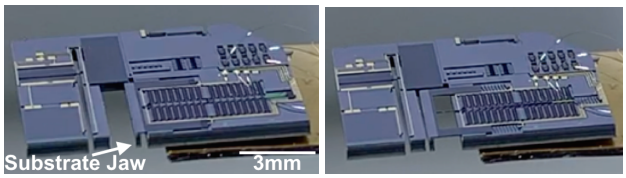

Figure 6: Gripper B opening and closing 1mm. Left – Open jaw. Right – Closed jaw.

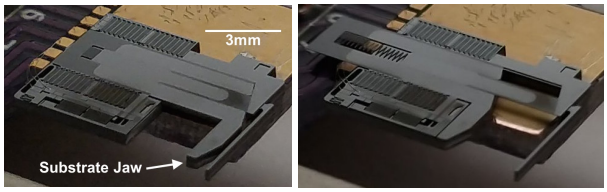

Figure 7: A redesigned gripper D (with no gold) opening and closing 3mm. The gripper is attached and wirebonded to a custom MEMS breakout board. Notice the shuttle is wider than gripper B's shuttle. Left – Open jaw. Right – Closed jaw.

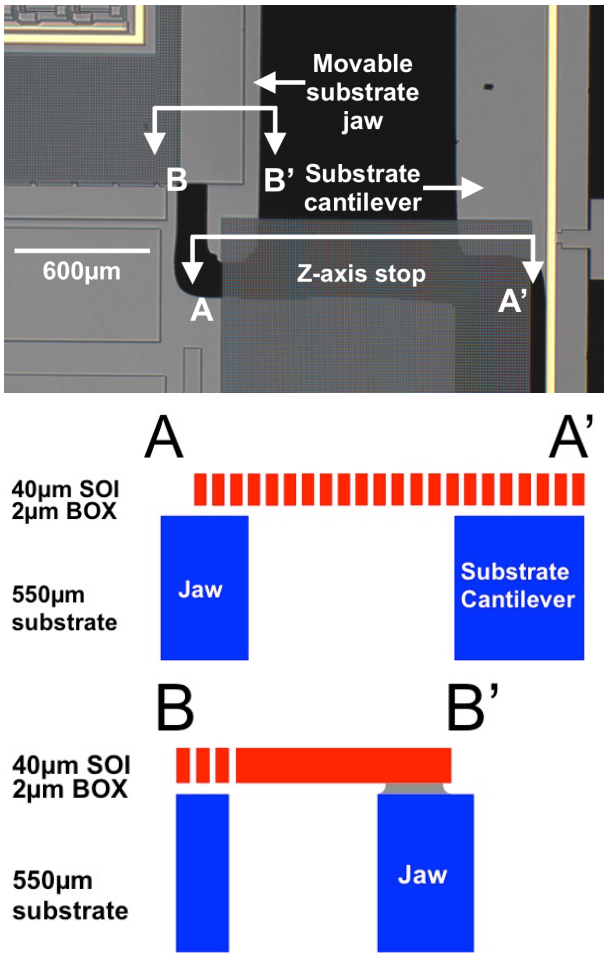

Figure 8: Top – Gripper B's jaw, substrate cantilever attached to its sensors, and z-axis stop. Bottom – Corresponding cartoon cross sections. A-A' shows the substrate jaw beneath the SOI z-axis stop. B-B' shows the substrate jaw attached to the SOI structure connected to the motor output shuttle.

Capacitive and Contact Sensing

On-chip capacitive finger arrays and resistive pull-up contact sensors as shown on gripper B (Figure 3) can be used to detect when an object is gripped. Figure 9 shows the circuit configurations used to read out the sensor outputs. The contact sensor creates up to a 0.5V change in the output of the leftmost circuit when using a 3V excitation supply voltage. The contact resistance is large (above 10MΩ) due to silicon-silicon sidewall contact of the engaged contact sensor. The pullup resistor is on chip and is on the order of 5MΩ. The contact sensor is also a limit stop determining the maximum displacement of the capacitive sensor.

Capacitance change (measured with an Analog Devices AD7746 evaluation board) and voltage vs. deflection are shown in Figure 10. The DRIE undercut at the top of the capacitive sensor fingers was measured to be 0.25µm using an SEM. The capacitance change vs. deflection theory fit assumes 89 degree DRIE sidewalls and an additional 1µm increase in the gap due to the depletion region caused by the fingers being made from lightly doped silicon. A 1 Vpp, 10kHz sine wave was

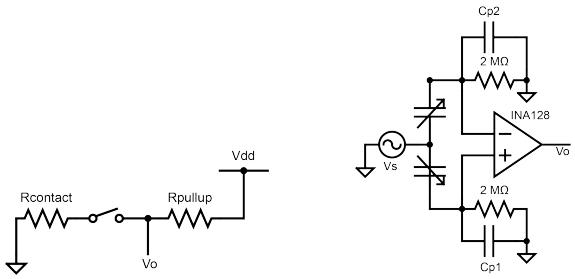

Figure 9: Left – The circuit used to sense when the contact sensor closed. Right – The circuit used to measure voltage vs. deflection of the capacitive sensor.

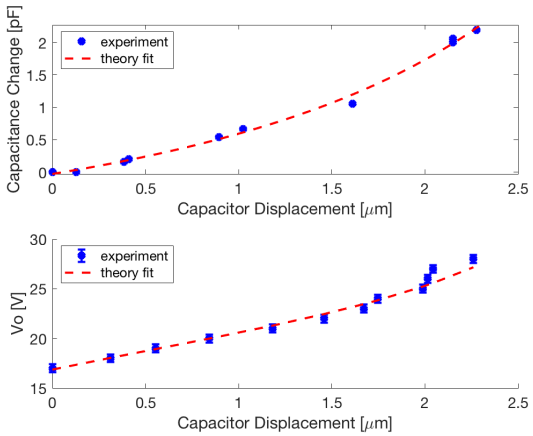

Figure 10: Measured capacitance change vs. deflection and measured voltage vs. deflection of the capacitive sensor on gripper B.

used as the excitation voltage, Vs. An INA128 amplifier with a gain of 167 was used to filter out noise and amplify the output signal. The values of Cp1 (24pF) and Cp2 (13pF) used for the theory fit were determined by doing a least squares error minimization of the data to the circuit's transfer function. Using this configuration, the output voltage Vo was measured and the capacitor displacement was measured optically with submicron resolution. The minimum detectable change in the capacitive sensor is less than 0.5µm.

While the capacitive and contact sensors displace less than 3µm, they are attached to a larger substrate cantilever structure (Figure 8) designed to displace up to 15µm. This substrate cantilever will displace as the gripper closes its jaw on an object, and its displacement is a function of the gripping force. At 15µm of displacement, the substrate cantilever exerts 15mN of force. The system should thereby be able to detect forces from 0 to 15mN, and sense individual 2µm steps of the electrostatic inchworm motor when gripping an object.

Z-Axis Stop

Figure 8 shows gripper B's z-axis stop and its cross section, inspired by [8]. The z-axis stop prevents the jaw from popping out of plane in the direction normal to the SOI surface. The stop is made from an SOI cantilever beam designed to be able to displace at least 1mm before fracturing. The purpose of the stop is to increase the robustness of the gripper by preventing SOI structures

attached to the jaw from shattering if the jaw is unintentionally displaced in the positive z-direction.

Gripping Objects

Gripper design B can successfully grab, hold on to, and release macroscopic objects. Figure 11 shows the gripper actively holding a 0.2 gram through-hole resistor. After gripping the resistor and removing power to the motor, the jaw's restoring springs fully retracted the jaw allowing the resistor to fall. This also confirmed that the gripping force was due to the jaw closing, and not electrostatic attraction, surface tension, or other forces that are predominant at such small scales.

CONCLUSION AND FUTURE WORK

Four different MEMS grippers have been designed and tested. Gripper B, the most successful design, is capable of displacing its jaw 1mm, gripping and releasing macroscopic objects, and contains working capacitive and resistive contact sensors. All four grippers contain a motor capable of producing 15mN of force at an estimated 0.3mW, and all contain onboard capacitive and resistive contact sensors. Grippers A and D have also been shown to move their jaws up to 2mm and 3mm, respectively, but have not yet successfully gripped an object. Gripper C had a working sensor platform, but needs further redesign before it can be actuated.

Future work includes gripping objects heavier than 0.2 grams with fully integrated force feedback. Additionally, all four grippers can be redesigned with increased jaw displacements and increased sensor sensitivity. Finally, integrating a gripper into a microrobotic platform [9] will enhance its capabilities when interacting with its environment.

Figure 11: The gripper is holding a 0.2 gram through-hole resistor. After the jaw is opened, the resistor falls.

ACKNOWLEDGEMENTS

This work was financially supported by the DARPA SHRIMP program, the National Science Foundation, and the Berkeley Sensor & Actuator Center. Devices were fabricated in the UC Berkeley Marvell Nanofabrication Laboratory.

REFERENCES

[1] A. Dochshanov, M. Verotti, and N. P. Belfiore, "A Comprehensive Survey on Microgrippers Design: Operational Strategy," *J. Mech. Des*, vol. 139, no. 7, Jul. 2017.

[2] T. Chen, L. Chen, L. Sun, and X. Li, "Design and fabrication of a four-arm-structure MEMS gripper," *IEEE Transactions on Industrial Electronics*, vol. 56, no. 4, pp. 996–1004, 2008.

[3] Femtotools.com. (2019). *FT-G Force Sensing Microgripper*. [online] Available at: https://www.femtotools.com/products/ft-mta03/accessories/ft-g-force-sensing-microgripper [Accessed 17 Nov. 2019].

[4] A. AbuZaiter, M. Nafea, and M. S. M. Ali, "Development of a shape-memory-alloy micromanipulator based on integrated bimorph microactuators," Mechatronics, vol. 38, pp. 16–28, 2016.

[5] X. Sun, W. Chen, S. Fatikow, Y. Tian, R. Zhou, J. Zhang, and M. Mikczinski, "A novel piezo-driven microgripper with a large jaw displacement," *Microsystem Technologies*, vol. 21, no. 4, pp. 931–942, 2015.

[6] C. B. Schindler, J. T. Greenspun, H. C. Gomez, and K. S. Pister, "A jumping silicon microrobot with electrostatic inchworm motors and energy storing substrate springs," in *2019 20th International Conference on Solid-State Sensors, Actuators and Microsystems & Eurosensors XXXIII (TRANSDUCERS & EUROSENSORS XXXIII)*. IEEE, 2019, pp. 88–91.

[7] I. Penskiy and S. Bergbreiter, "Optimized Electrostatic Inchworm Motors Using A Flexible Driving Arm," *Journal of Micromechanics and Microengineering*, vol. 23, no. 1, p. 015018, 2012.

[8] B. Kilberg, D. Contreras, J. Greenspun, H. Gomez, E. Liu, and K. S. J. Pister, "MEMS Airfoil With Integrated Inchworm Motor and Force Sensor," in Hilton Head Workshop on Solid-State Sensors, Actuators, and Microsystems, 2018.

[9] D. S. Contreras and K. S. J. Pister, "A Six-Legged MEMS Silicon Robot Using Multichip Assembly," in Hilton Head Workshop on Solid-State Sensors, Actuators, and Microsystems, 2018.

CONTACT

*Contributed equally
C. B. Schindler; craig.schindler@berkeley.edu
H. C. Gomez; gomezhc@berkeley.edu